

Diffraction pattern of triangular grating in the resonance domain

Tetsuya Hoshino, Saswatee Banerjee, Masahide Itoh

*Institute of Applied Physics, University of Tsukuba,
1-1-1 Tennoudai, Tsukuba 305-8577, Japan*

hoshino@gabor.bk.tsukuba.ac.jp

Toyohiko Yatagai

*Institute of Applied Physics, University of Tsukuba,
1-1-1 Tennoudai, Tsukuba 305-8577, Japan*

*Center for Optical Research and Education, Utsunomiya University,
7-1-2 Yoto, Utsunomiya, Tochigi 321-8585, Japan*

We propose a combination of ray optics and Fraunhofer multiple-slit diffraction theory for calculating the two-dimensional triangular periodic grating in the resonance domain. The peak of the envelope pattern of angular distribution of diffraction efficiency is calculated by ray optics, while the peak width is calculated using Fraunhofer theory. It was clarified, using rigorous coupled wave analysis and a nonstandard-finite-difference time-domain method, that the envelope pattern of the diffraction of the grating could be calculated easily and understood intuitively for the design of displays and lighting. © 2008 Optical Society of America

OCIS codes: 050.1950, 050.1970, 050.5745, 230.1950, 230.3990, 240.3990.

1. Introduction

Optical components having antireflection or polarization selection properties are useful for displays and lighting represented by liquid crystal displays (LCDs) and light emitting diodes (LEDs) [1–3].

In this study, we used gratings in the resonance domain having periods ranging from one to several tens of wavelengths. Triangular gratings are promising for applications requiring antireflection, polarization selection and spreading, which are best explained in terms of diffractive optics rather than ray optics [4–6]. However, the diffractive optics of the grating are difficult to understand intuitively.

When the value (period Λ)/(wavelength λ) ≥ 20 , physical optics according to Fresnel and Snell's laws can explain the spreading pattern of the prism array. When $\Lambda/\lambda \leq 0.5$, the effective medium theory can explain the diffraction pattern of the grating by averaging refractive indices of the layer of surface relief [7]. Those theories for the two range of Λ/λ enable us to understand the optical characteristics easily.

However, when $1 \leq \Lambda/\lambda \leq 10$, the behavior of the diffraction light is difficult to understand intuitively. In this region, calculation is possible by using a complex simulation such as rigorous coupled wave analysis (RCWA) [8,9] or the beam-propagation method (BPM) [10, 11].

Calculation by rigorous diffractive optics is possible only if the period is of the order of the wavelength and only a few wavelengths are to be calculated [12], since a longer period results in a longer calculation time. For example, the extraction efficiency of LEDs is usually calculated by ray optics [7, 13, 14].

BPM and other scalar diffraction theories [10, 15–17] are also widely used for large-scale calculations, for example calculation of light waveguides, and predict the loss by absorption and scattering. However, they do not yield intuitive solutions based on simple analytical equations. In comparison, it is easy to use ray optics to calculate gratings having a large

modulation in relative permittivity. It is also easy to estimate reflection as well as transmission using ray optics. Moreover, ray optics are intuitive, which is useful for improving the design of the grating [18–20].

One intuitive theory is Fraunhofer’s single slit diffraction: diffracted light spreads in inverse proportion to the width of the slit [21,22]. This theory is applicable to an aperture in a plane screen, but not to a surface relief grating.

As mentioned above, ray optics are easy to apply and are a powerful design tool, if available. We have attempted to calculate triangular gratings in the resonance domain by modifying ray optics. Specifically, we tested a combination of ray optics and Fraunhofer approximation. We considered the factors that differentiate the results of physical optics and diffractive optics, and developed a method to modify the results of ray optics to fit the results of diffractive optics. The modification is explained easily and intuitively. Thus we exploited the way to estimate the diffraction pattern of the surface relief grating in the resonance domain easily for the first time.

2. Simulation method

The diffraction efficiency of the grating was computed using rigorous coupled wave analysis (RCWA), and the electric field was computed with nonstandard finite-difference time-domain (NS-FDTD) algorithms, for a grating with an isosceles triangle profile.

RCWA was performed using *DiffractMODTM* 1.5 (RSoft Design Group, Ossining, NY, USA). The NS-FDTD program was run under *MathCADTM* 2004 (MathSoft Engineering and Education, Inc., Cambridge, USA) [23–25]. The detailed calculation conditions are described in a previous paper [6]. The calculated grating is shown in Fig. 1. The light travels from air to the grating, which is defined as case A. To generalize the situation, case B, in which the light travels in the opposite direction to that of case A, is also considered.

3. Fitting of the envelope pattern of diffraction pattern

We have previously calculated the total reflectivity of the triangular periodic grating of surface relief [5,6]. Here, the total reflectivity is the sum of all the diffraction efficiencies of reflection. We also calculated the diffraction efficiency to observe the change in the peak of the diffraction pattern in the TE and TM modes [5]. The incident plane wave polarization of the TE mode is perpendicular to the plane of incidence. We newly explain the effect of Λ/λ on the width of the peak of the diffraction pattern using the relationship between Λ/λ and diffraction efficiency.

The similarity between the angular distributions for different Λ/λ may be evaluated by the following factors. (1) Deviation of the peaks of angular distributions of the two Λ/λ . (2) Different broadening of the peaks of two Λ/λ . As mentioned below, the diffraction pattern

did not usually change significantly as a function of Λ/λ . Let i be the diffraction order. When the parameter $i\lambda/\Lambda$ of the peak does not change, the angle θ of the peak of the envelope pattern of diffraction is constant against Λ/λ [5]. This concept can also be applied to three dimensions as shown in the appendix. If Λ becomes large enough, the peak position of diffraction pattern is predicted by ray optics. It turns out that ray optics can be used to determine θ of the peak of the envelope. The problem then becomes how to determine the width of the peak. It is known that the diffraction pattern of a periodic single slit can be explained by the diffraction angle and its envelope pattern [21, 26]. We calculated the angular distribution of a triangular grating by RCWA and compared its peak width with that calculated by the Fraunhofer single-slit diffraction theory.

Equation (1) gives the Fraunhofer single-slit diffraction pattern [21].

$$I_T(\theta) = A^2 \Lambda_2^2 [\sin\{\pi\Lambda_2(\sin\theta - \sin\theta')/\lambda_2\} / (\pi\Lambda_2(\sin\theta - \sin\theta')/\lambda_2)]^2, \quad (1)$$

where $I_T(\theta)$ is the angular distribution of diffraction intensity, Λ_2 is the slit width, λ_2 is the wavelength, and A is a constant. θ' is the incidence angle and θ is the angle of the peak of the envelope pattern of diffraction. Using this equation, we estimated the peak width of the envelope curve of the diffraction pattern for various wavelengths and aspect ratios. When the refractive index is n , λ_2 is substituted by $n\lambda_2$ in case A. The parameters A , θ' , and λ_2 were then changed so that the peak width agrees with that of RCWA.

4. Results of angular distribution of diffraction efficiency

We consider the angular distribution of the diffraction efficiency which varies with the parameters of Λ/λ , d/Λ and θ . The peak position and peak width are to be checked against Λ/λ .

Figure 2 shows the transmissivity or reflectivity of light for various conditions to compare two Λ/λ as standard diffraction patterns. The diffraction pattern did not change significantly with Λ/λ . The top chart in Fig. 2 has peaks at $\pm 30^\circ$, which are the same as that of ray optics. In Fig. 3, the angular distribution of the transmitted light is shown, indicating the effects of Λ/λ . The calculation conditions include the incident angle 0° , the direction of incident light indicated by case A or B, the polarization TE and the refractive index of the grating of 1.5. Λ/λ was varied for comparing the results.

Equation (1) was used to curve fit the data given in the following tables using the Fraunhofer single-slit diffraction theory. The curve fitting results for Fig. 3 are shown in Table 1. λ and Λ are used for RCWA calculations, and λ_2 and Λ_2 are used for the fitting parameters for Fraunhofer theory.

In Fig. 4, Λ/λ is varied for a grating of aspect ratio 2. The envelope pattern of $\Lambda/\lambda = 4.5$ is very different from that of $\Lambda/\lambda = 9.1$ and 22.7. It seems that the two peaks coupled

together for Λ/λ of 4.5 and yielded one peak around 0° . Table 2 corresponds to Fig. 4. $I_T(\theta)$ with parameters of the table agreed with each envelope in the Fig. 4.

From the above results, the apparent ratio of the period $(\Lambda/\lambda)(\lambda_2/\Lambda_2)$ is more than 1 and is almost constant when Λ/λ is greater than 9.

In Fig. 5 and Table 3, d/Λ is changed. As d/Λ becomes larger, $(\Lambda/\lambda)(\lambda_2/\Lambda_2)$ becomes larger. In Fig. 5(b), Λ/λ of 9.1 and 22.7 are compared for d/λ of 2.5 and 3, respectively.

As shown above, we can see the effect of diffraction gives different results from those of ray optics. As Λ/λ increases, the angle of the peak approaches that of physical optics. The peak with Λ/λ of 22.7 is close to the peak with the Λ/λ of physical optics.

In Fig. 6 and Table 4, the incident angle θ' is varied. The angular distribution of θ' from 0 to 30° and that of θ' from 50 to 70° may be attributed to different groups as their peak widths are very different.

In Fig. 7 and Table 5, the incident angle is 20° and Λ/λ is varied. The angular distribution of the transmitted light is shown in Fig. 7. The direction of the incident light is case B, the polarization is TE, and d/Λ is 1. The angle of the peak is close to 90° . Some of the diffraction angles that contribute to the diffraction efficiency may exceed 90° , when we consider the peak width of Fraunhofer diffraction. This explain the fact that the angular distribution and total transmissivity are significantly different for different Λ/λ in Table 5. It should be noted that the total transmission is the sum of all diffraction efficiencies of transmission.

When Λ/λ is 9.1 or 22.7, the aspect ratio is 1 and the angle of incidence is 0° , the light direction is that of case B, the polarization is TM, and the angular distributions of transmission are similar, but those of reflection are not necessarily so. The reflective angular distribution of the diffraction efficiency varies greatly by wavelength if θ is less than 15° . In that case, the maximum diffraction efficiency is less than 10 %. For example, when the angle of incidence is 0° , there are peaks at $\pm 20^\circ$ and $\pm 50^\circ$ for $\Lambda/\lambda = 5$. However, the peaks at $\pm 50^\circ$ seem to disappear for $\Lambda/\lambda = 10$. The maximum diffraction efficiency in this case is 2%.

5. Results of electric field distribution

To determine the diffraction pattern for one groove, the electric field was calculated. The light direction is case A and θ' is 0° . The calculated results of the electric field distribution are shown in Fig. 8. The axes of electric field are shown by X and Y in Fig. 8(a). The total calculation space is $100\lambda \times 45.5\lambda$ along the X and Y axes, respectively. The boundary condition on the left and right are periodic, the top and bottom boundaries are absorbing, the refractive index of the upper side is 1 and that of the down side is 1.5, and Λ/λ is 9.1. In Fig. 8(b), the dotted line is the grating and it can be seen that there are two stripes of the scattered light.

6. Discussion

We did not directly compare the results of ray optics and diffractive optics, but rather we compared the results of Λ/λ of 22.7 with those of Λ/λ of 9.1 and 4.5. As Λ/λ increases, the pattern approaches that of ray optics. We assume that when Λ/λ is 22.7, the angular distribution is close to that calculated by physical optics. That is, the peak position and width are similar. In the appendix, the equation for the diffraction efficiency for three dimensions is derived. The equation suggests that the peak of diffraction pattern does not change against λ . Moreover, single-slit diffraction was used to calculate the broadening of the peak. Finally, we show a way to calculate the diffraction pattern.

The index of the peak width is Λ_2/λ_2 , and $(\Lambda/\lambda)/(\Lambda_2/\lambda_2)$ is almost constant in Tables 1 and 2 if Λ/λ is greater than 9. This implies that we can assume the triangular grating behaves as a single-slit with a width proportional to the period. Figure 8 shows the electric field of light diffracted by one grating. We can see two diffraction stripes from the groove. These two stripes correspond to the two peaks in Fig. 2 and support the idea that a groove functions as a slit. This result can be easily understood if the base of the groove functions like a slit.

The main differences between the results for Λ/λ of 9.1 and 22.7 are as follows: (1) different peak positions of the angular distribution, (2) broadening of angular distribution by the single-slit effect for Λ/λ of 9.1, and (3) reduction in the total reflectivity for Λ/λ of 22.7 [6].

In the above list, (1) is the case when the number of peaks is different by Λ/λ , and the grating with Λ/λ of 9.1 has the other peak than that with Λ/λ 22.7. The peak positions are different especially when transmission or reflection is less than 5% (3) is the case when the longer period reduces the reflectivity. (1) and (3) can be neglected, since the difference of diffraction efficiency is small. Case (2) is shown in Figs. 2 and 3 for a typical example, and it further highlights the following two differences between Λ/λ of 9.1 and 22.7: (2a) Coupling of two peaks, such as in Figs. 4 and 5(b), and (2b) reduction in reflectivity due to the reduction in the diffraction efficiency caused by the diffraction angle exceeding 90° , as in Fig. 7 and Table 5. Thus, we have shown the difference between the results of ray optics and diffractive optics in the resonance domain.

The recipe for cases (2a) and (2b) is as follows: (2a) For the coupling of two peaks, the solution is to simulate these as a single peak. As shown in Table 1, $(\Lambda/\lambda)/(\Lambda_2/\lambda_2)$ is not far from 1. (2b) This difference can be corrected by disregarding diffraction at angles greater than 90° . As shown in Fig. 7, the envelope pattern does not deviate from the single-slit Fraunhofer diffraction even in this case.

Thus, for the angular distribution and the total reflectivity, the case wherein the characteristics are not the same for a similar shape of the grating is clarified.

As discussed above, the width of the peak can be predicted by Λ/λ using single-slit Fraun-

hofer diffraction. Moreover, the angle of the peak is calculated by ray optics. Thus, the envelope pattern of the grating in the resonance domain can be predicted using ray optics and the above results.

The diffraction efficiency of each diffraction order is calculated using the theory of multiple-slit Fraunhofer diffraction [21]. Each diffraction angle is determined from θ' and Λ automatically using the relationship between i , λ , Λ , θ , θ' and refractive index [21]. The envelope of the diffraction pattern and the diffraction angle gives the diffraction efficiency of each order. The combination of ray optics and multiple-slit Fraunhofer diffraction theory enable us to calculate the diffraction efficiency .

7. Conclusions

For the angular distribution of the diffraction efficiency of the triangular grating in the resonance domain, the peak position and width of the envelope pattern were calculated by ray optics and Fraunhofer diffraction theory. The exceptional cases, which cannot be calculated simply by using these theories, were classified into three cases, wherein the angular distribution changes significantly with the period/wavelength. (1) The peak width is larger than the difference between the two peaks calculated by ray optics; (2) the incident light is diffracted near the vertical to the vector of 0th order diffraction; and (3) the diffraction angle is close to 90° . Even for these cases, a minor modification enables us to calculate the grating easily by using a combination of ray optics and Fraunhofer approximation, which yields insights into the intuitive analysis of the light paths for the first time.

Appendix A

As mentioned in the introduction, the diffraction efficiency against Λ/λ is important to the design of the grating in the resonance domain. To understand the behavior of the diffraction pattern vs. Λ/λ in two dimensions, we have restructured the equations for the derivation of the electric field amplitude in the rigorous coupled-wave equations in Moharam and Gaylord's paper [5]. We showed that when the variables of the diffraction efficiency were i , λ , Λ and d , the independent parameters were only $i\lambda/\Lambda$ and d/λ . In this section we will show this theoretical frame work is also applicable to three dimensions. It is important to be able to apply this frame work to three dimensions, because calculation time by RCWA is much the longer for three dimensions than for two dimensions.

The three-dimensional geometry of the grating with incidence and diffraction is shown in Fig. 9 [9]. \mathbf{k}_1 is the vector of the incident light, \mathbf{k}_3 is the vector of the transmitted light, and \mathbf{K} is the grating vector.

A linearly polarized electromagnetic wave is obliquely incident at an angle α on a slanted-fringe planar grating with a slant angle of ϕ bounded by two different homogeneous media.

The planar grating has an arbitrary direction of periodicity (direction of grating vector \mathbf{K}). In the analysis presented here, the following geometry is used: (1) The boundary normals are in the z direction, (2) the grating vector is in the $x - z$ plane, and (3) the plane of incidence makes an angle of δ with respect to the x axis. The modulated region ($0 < z < d$) contains a mixed amplitude and phase grating.

The grating vector is given by

$$\begin{aligned}\mathbf{K} &= K_x \hat{x} + K_z \hat{z} \\ &= K \sin \phi \hat{x} + K \cos \phi \hat{z}.\end{aligned}\tag{A1}$$

The normalized total vector electric field in region 3 ($z > d$) may be expressed as

$$\mathbf{E}_3 = \sum_i \mathbf{T}_i \exp[-j\mathbf{k}_{3i} \cdot (\mathbf{r} - d\hat{z})],\tag{A2}$$

where j is $(-1)^{1/2}$, d is the thickness of the grating and $\mathbf{r} = x\hat{x} + y\hat{y} + z\hat{z}$ with $\hat{}$ denotes a unit vector. \mathbf{T}_i is the normalized vector electric field of the i th forward-diffracted (transmitted) wave in region 3 with wave vector \mathbf{k}_{3i} .

In the general three-dimensional vectorial problem under consideration, all the electric and magnetic space-harmonic fields are coupled to each another. Maxwell's theory gives two equations for the magnetic field vector and electric field vector [9]. The electric and magnetic fields may be expressed as Fourier expansions in terms of the space harmonic field, and substituting the Fourier expansions into the above two equations results in a set of four first-order coupled-wave equations [9]. These are differential equations in terms of $S_{xi}(z)$, $S_{yi}(z)$, $U_{xi}(z)$ and $U_{yi}(z)$, respectively. Here, $\mathbf{S}_i(\mathbf{z})$ and $\mathbf{U}_i(\mathbf{z})$ are the i th space-harmonic vector with normalized amplitudes. $S_{xi}(z)$, $S_{yi}(z)$, $U_{xi}(z)$ and $U_{yi}(z)$ are the components of the vector. For example, the differential equation of $S_{xi}(z)$ is given by:

$$\begin{aligned}\lambda \frac{dS_{xi}(z)}{dz} &= -j\{2\pi i\lambda/\Lambda \sin \phi S_{xi}(z) - (\varepsilon_I^{1/2} \sin \alpha \cos \delta \\ &\quad - i\lambda/\Lambda \sin \phi) \sum_p a_{i-p} [2\pi \varepsilon_I^{1/2} \sin \alpha \sin \delta U_{xp}(z) \\ &\quad - (2\pi \varepsilon_I^{1/2} \sin \alpha \cos \delta - 2\pi p\lambda/\Lambda \sin \phi) U_{yp}(z)] + 2\pi U_{yi}(z)\}.\end{aligned}\tag{A3}$$

Here, α is the angle between \mathbf{k}_1 and the z axis, and δ is the angle between the plane of incidence and the x axis as shown in Fig. 10. ε_I is the relative permittivity in region 1. $p = i - h$ and a_h are the h th coefficient of the Fourier expansion of $\varepsilon^{-1}(x, z)$ in the form:

$$\varepsilon^{-1}(x, z) = \sum_h a_h \exp(jh\mathbf{K} \cdot \mathbf{r}).\tag{A4}$$

Here, $\varepsilon(x, z)$ is the periodic complex relative permittivity.

Let the parameter be i, λ, Λ and d . It is clear that all the coefficients of the right-hand side terms of (A3) are expressed only by $i\lambda/\Lambda$, $p\lambda/\Lambda$ and d/λ , where $p\lambda/\Lambda$ is the coefficient of S_{xp} , U_{yp} etc. The coefficients of the other three differential equations are also expressed in a similar way. When p is equal to i , $(2\pi p\lambda/\Lambda \sin \phi)U_{yp(z)}$ has the coefficient $i\lambda/\Lambda$. Due to the contribution from p , other than i , the coefficients on the right side also has the parameter λ/Λ , which may make the dependency of reflectivity and transmissivity on $i\lambda/\Lambda$ more complex.

These four differential equations can be written in matrix form as:

$$\lambda \dot{\mathbf{V}} = \mathbf{A} \mathbf{V}, \quad (\text{A5})$$

where \mathbf{V} and $\dot{\mathbf{V}}$ are the column vectors of the matrix form, and \mathbf{A} is the system matrix in the differential equation [9]. \mathbf{A} has parameters $i\lambda/\Lambda$, $p\lambda/\Lambda$ and d/λ .

The solutions of the coupled-wave equations for $S_{xi}(z)$ may be expressed as:

$$S_{xi}(z) = \sum_m C_m \omega_{1,im} \exp(\lambda_m z / \lambda), \quad (\text{A6})$$

where C_m is the unknown constant to be determined from the boundary conditions, and $\omega_{1,im}$ and λ_m are eigenvectors and eigenvalues of the matrix \mathbf{A} . $S_{yi}(z)$, $U_{xi}(z)$ and $U_{yi}(z)$ are expressed in the same way [9].

The amplitude of the diffracted fields \mathbf{R}_i and \mathbf{T}_i (together with C_m) are calculated by matching the tangential electric and magnetic fields at the two boundaries $z = 0$ and $z = d$ [9]. It turns out that coefficients of $|\mathbf{R}_i|^2$ and $|\mathbf{T}_i|^2$ are expressed only by $i\lambda/\Lambda$ and d/λ according to the boundary conditions.

The diffraction efficiency is defined as the ratio of the component of the real power carried by the diffracted wave normal to the boundary (z component) to the corresponding component of the real power associated with the incident wave. That is,

$$DE_{1i} = -\text{Re}[(k_{z1i})/(k_1 \cos \alpha)] |\mathbf{R}_i|^2, \quad (\text{A7})$$

$$DE_{3i} = \text{Re}[(k_{z3i})/(k_1 \cos \alpha)] |\mathbf{T}_i|^2, \quad (\text{A8})$$

where wave vector \mathbf{k}_{1i} is the i th backward-diffracted (reflected) wave in region 1 and \mathbf{k}_{3i} is the i th forward-diffracted (transmitted) wave in region 3. k_{z1i} and k_{z3i} are the z components of the vectors and k_1 is the size of the vector. k_1/k is $\varepsilon_{\text{I}}^{1/2}$. k_{z1i}/k is given by

$$k_{z1i}/k = \varepsilon_{\text{I}}^{1/2} [(\varepsilon_l/\varepsilon_{\text{I}})^2 - (\sin \alpha \cos \delta - i\lambda/\Lambda \sin \phi)^2 - (\sin \alpha \sin \delta)^2]^{1/2}, \quad (\text{A9})$$

where $l = 1, 3$ (the region index), α is the angle between \mathbf{k}_1 and z axis. DE_{1i} and DE_{3i} are the diffraction efficiencies of the backward-diffracted and forward-diffracted waves in the directions \mathbf{k}_{1i} and \mathbf{k}_{3i} , respectively. DE_{1i} and DE_{3i} have coefficients whose parameter is $i\lambda/\Lambda$. Moreover, \mathbf{R}_i and \mathbf{T}_i have parameters $i\lambda/\Lambda$, λ/Λ and d/λ . Thus, $i\lambda/\Lambda$ and d/λ are important as parameters.

Next, we consider the surface relief grating with a striped shape. The projected figure is Fig. 1. d is the depth of the grating. We are going to show the vector diffraction theory described in this appendix can also be applied to surface-relief gratings as mentioned briefly by Moharam and Gaylord [9]. The triangular surface relief grating can be decomposed into planar gratings as shown in Fig. 11. Each layer has a first-order state equation such as Eq. (A3) [8]. We can solve the equation by using the boundary condition for each layer. The independent parameters become $i\lambda/\Lambda$, λ/Λ and d/λ in the same way.

Which term in the above equations contributes most to the broadening? The candidate is $a_{i-p}(2\pi\varepsilon_I^{1/2} \sin \alpha \cos \delta - 2\pi p\lambda/\Lambda \sin \phi)U_{yp}(z)$ in Eq. (A3). It includes the parameter Λ and the intercrossing term for the diffraction order. If there is not this term, we can see that the independent parameters becomes only $i\lambda/\Lambda$ and d/λ . Then we check the effect of this term on the diffraction efficiency.

As $|i - p|$ becomes larger, a_{i-p} becomes small. For example, we think a rectangular grating with the period of 2π and ϕ of $\pi/2$. In Eq. (A4) $a_0 = \text{constant}$ and $a_h = c \times b_h$ for $h \neq 0$. Here, c is constant, and b_h is $2j/(\pi h)$ for even h and zero for odd h . In this case a_{i-p} is roughly proportional to $1/|i - p|$.

Then, p near i is important in the term of Eq. (A3). It turns out that the important independent parameters are $i\lambda/\Lambda$ and d/λ . If the influence of $i\lambda/\Lambda$ on the diffraction efficiency is much larger than that of d/λ , diffraction efficiency is controlled by $i\lambda/\Lambda$.

Moreover, $i\lambda/\Lambda$ can be connected to the diffraction angle θ_i through Eq. (A10) [21]. Here, n_I is the refractive index of region 1 and n_{III} is that of region 3.

$$n_{III} \sin(\theta_i) - n_I \sin(\theta') = i\lambda/\Lambda. \quad (\text{A10})$$

Then, the diffraction efficiency and the diffraction angle are dominated by $i\lambda/\Lambda$, when the influence of $i\lambda/\Lambda$ on the diffraction efficiency is much larger than that of d/λ . At that time, same $i\lambda/\Lambda$ brings same diffraction efficiency and same diffraction angle, which gives invariant diffraction pattern against wavelength shift [5].

Finally, Eq. (A3) suggests that the angle of the peak of the envelope of diffraction pattern is almost constant against wavelength.

Acknowledgements

The authors thank Dr. J. B. Cole for his NS-FDTD program.

References

1. M. F. Weber, C. A. Stover, L. R. Gilbert, T. J. Nevitt, and A. J. Ouderkirk, “Giant birefringent optics in multilayer polymer mirrors,” *Science* **287**, 2451–2456 (2000).
2. A. M. Nuijs and J. J. L. Horikx, “Diffraction and scattering at antiglare structures for display devices,” *Appl. Opt.* **33**, 4058–4068 (1994).
3. S. X. Jin, J. Li, J. Y. Lin, and H. X. Jiang, “InGaNOGaN quantum well interconnected microdisk light emitting diodes,” *Appl. Phys. Lett.* **77**, 3236–3238 (2000).
4. G. S. White and J. F. Marchiando, “Scattering from a V-shaped groove in the resonance domain,” *Appl. Opt.* **22**, 2308–2312 (1983).
5. T. Hoshino, M. Itoh, and T. Yatagai, “An antireflective grating in the resonance domain for displays,” *Appl. Opt.* **46**, 648–656 (2007).
6. T. Hoshino, S. Banerjee, M. Itoh, and T. Yatagai, “Design of a wavelength independent grating in the resonance domain,” *Appl. Opt.* **46**, 7948–7962 (2007).
7. T.-X. Lee, C.-Y. Lin, S.-H. Ma, and C.-C. Sun, “Analysis of position-dependent light extraction of GaN-based LEDs,” *Opt. Express* **13**, 4175–4179 (2005).
8. M. G. Moharam and T. K. Gaylord, “Diffraction analysis of dielectric surface-relief gratings,” *J. Opt. Soc. Am. A* **72**, 1385–1392 (1982).
9. M. G. Moharam and T. K. Gaylord, “Three-dimensional vector coupled-wave analysis of planar-grating diffraction,” *J. Opt. Soc. Am.* **73**, 1105–1112 (1983).
10. M. D. Feit and J. A. Fleck, “Light propagation in graded-index optical fibers,” *Appl. Opt.* **17**, 3990–3998 (1978).
11. J. V. Roey, J. van der Donk, and P. E. Lagasse, “Beam-propagation method: analysis and assessment,” *J. Opt. Soc. Am.* **71**, 803–810 (1981).
12. S. R. Park, O. J. Kwon, D. Shin, S.-H. Song, H.-S. Lee, and H. Y. Choi, “Grating micro-dot patterned light guide plates for LED backlights,” *Opt. Express* **15**, 2888–2899 (2007).
13. K. Kalil, M. Shingo, K. Tatsuya, and M. Toshiyuki, “Backlight Unit with Double Surface Light Emission Using a Single Micro-Structured Light-Guide Plate,” *IEICE transactions on electronics* **E87-C**, 1954–1961 (2004).
14. T.-X. Lee, K.-F. Gao, W.-T. Chien, and C.-C. Sun, “Light extraction analysis of GaN-based light-emitting diodes with surface texture and/or patterned substrate,” *Opt. Express* **15**, 6670–6676 (2007).
15. S. Ahmed and E. N. Glytsis, “Comparison of beam propagation method and rigorous coupled-wave analysis for single and multiplexed volume gratings,” *Appl. Opt.* **35**, 4426–4435 (1996).
16. S. Mellin and G. Nordin, “Limits of scalar diffraction theory and an iterative angular

- spectrum algorithm for finite aperture diffractive optical element design,” *Opt. Express* **8**, 705–722 (2001).
17. J. E. Harvey, A. Krywonos, and D. Bogunovic, “Nonparaxial scalar treatment of sinusoidal phase gratings,” *J. Opt. Soc. Am. A* **23**, 858–865 (2006).
 18. G. H. Spencer and M. V. R. K. Murty, “General ray-tracing procedure,” *J. Opt. Soc. Am.* **52**, 672–678 (1962).
 19. W. C. Sweatt, “Describing holographic optical elements as lenses,” *J. Opt. Soc. Am.* **67**, 803–808 (1977).
 20. M. Testorf, “Perturbation theory as a unified approach to describe diffractive optical elements,” *J. Opt. Soc. Am. A* **16**, 1115–1123 (1999).
 21. M. Born and E. Wolf, *Principles of Optics, : Electromagnetic Theory of Propagation, Interference and Diffraction of Light* (Cambridge University Press, Cambridge, 1999), 7th ed.
 22. G. S. White and A. Feldman, “Diffraction from a shallow rectangular groove,” *Appl. Opt.* **20**, 2585–2589 (1981).
 23. J. B. Cole, S. Banerjee, and M. Haftel, “High accuracy nonstandard finite-difference time-domain algorithms for computational electromagnetics: applications to optics and photonics,” in “*Advances in the applications of nonstandard finite difference schemes*,” R. E. Mickens, ed. (World Scientific, 2006), pp. 89–189.
 24. J. B. Cole and S. Banerjee, “Applications of nonstandard finite difference models to computational electromagnetics,” *J. Diff. Eqns.* **9**, 1099–1112 (2003).
 25. J. B. Cole and S. Banerjee, “Improved version of the second-order mur absorbing boundary condition based on a nonstandard finite difference model,” in “*The 23rd Annual Review of Progress in Applied Computational Electromagnetics*,” (Applied Computational Electromagnetics, Verona, Italy, 2007), pp. 1531–1535.
 26. M. Ouyang, Y. Cao, H. Gao, J. Shi, J. Zhou, and D. Liu, “Analysis on polarization dependence of Fraunhofer diffraction by metallic grating with short period,” *Optics and Laser Technology* **40**, 201–207 (2008).

List of Figures and Tables

Fig. 1 (Color online) The shape of the triangular grating profile, and the definition of Λ , d , and ds . The fill factor is 0.5. The light direction for case A is shown. ds is assumed to be infinity. The refractive index n of the grating is 1.5.

Fig. 2 (Color online) Angular distribution of the diffraction efficiency for different polarization and light directions. Λ/λ is 9.1 or 22.7. The aspect ratio is 1. Though the diffraction efficiency is discrete, it is connected with the auxiliary line to make it intelligible. Fig. 3 (Color online) Angular distribution of the transmissive diffraction efficiency of the TE mode for case B for different Λ/λ . The aspect ratio is 1. The diffraction efficiency is connected with the auxiliary line to make it intelligible. Λ/λ is varied from 4.5 to 22.7.

Fig. 4 (Color online) Angular distribution of the transmissive diffraction efficiency of the TE mode for case A for different Λ/λ . The aspect ratio is 2. The diffraction efficiency is connected with the auxiliary line to make it intelligible. Λ/λ is varied from 4.5 to 22.7.

Fig. 5 (Color online) Angular distribution of the transmissive diffraction efficiency of the TE mode for different d/Λ for case A. The diffraction efficiency is connected with the auxiliary line to make it intelligible. (a) d/Λ is varied from 0.25 to 3. (b) d/Λ is 2.5 and 3, and Λ/λ is 9.1 and 22.7.

Fig. 6 (Color online) The incidence angle θ' is varied. The angular distribution of θ' from 0° to 30° and that of θ' from 50° to 70° may be attributed to different groups by their peak width.

Fig. 7 (Color online) The angular distribution of the transmitted light is shown. The incidence angle is 20° , the direction of the incident light is case B, the polarization is TE, d/Λ is 1, and Λ/λ was varied. The angle of the peak is near 90° . The angular distribution varies greatly with Λ/λ .

Fig. 8 (Color online) (a) The field for FDTD calculation and the grating. The black rectangular area is expanded into the area of (b). (b) The phase distribution of the scattered light in the TE mode and for case A. There is only one groove, unlike Fig. 1. The width of the groove is 9.1λ and the aspect ratio is 1.

Fig. 9 Geometry of forward-diffracted wave vectors showing the conical nature of diffraction. Forward-diffracted waves ($i = -1$ to $i = +2$) are indicated by the arrow. The light travels from region 1 ($z < 0$) to region 3 ($z > d$).

Fig. 10 A linearly polarized electromagnetic wave of wave vector \mathbf{k}_1

Fig. 11 The planar gratings resulting from the decomposition of the surface relief grating into N thin gratings.

Table. 1 The results of curve fitting for Fig. 3 by the Fraunhofer single-slit diffraction pattern for different Λ/λ in case B. Apparent ratio of the period is calculated by $(\Lambda/\lambda)(\lambda_2/\Lambda_2)$.

Table. 2 The results of curve fitting for Fig. 4 by Fraunhofer single-slit diffraction pattern for different Λ/λ and d/Λ in case A. The parameters are the same as in Fig. 1 and Eq. (1). The apparent ratio of the period is calculated by $(\Lambda/\lambda)(n\lambda_2/\Lambda_2)$.

Table. 3 The results of curve fitting for Fig. 5 by Fraunhofer single-slit diffraction pattern for different aspect ratios in case A. Λ/λ is 9.1. Apparent ratio of period is calculated by $(\Lambda/\lambda)(n\lambda_2/\Lambda_2)$.

Table. 4 The results of curve fitting for Fig. 6 by Fraunhofer single-slit diffraction pattern for different incidence angle in case A. Apparent ratio of period is calculated by $(\Lambda/\lambda)(n\lambda_2/\Lambda_2)$.

Table. 5 Total transmissivity of Fig. 7 as a function of Λ/λ . "Transmissivity" is the sum of the transmission diffraction efficiency.

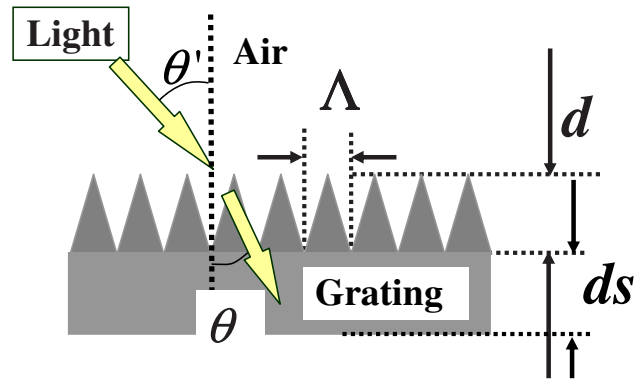


Fig. 1. (Color online) The shape of the triangular grating profile, and the definition of Λ , d , and ds . The fill factor is 0.5. The light direction for case A is shown. ds is assumed to be infinity. The refractive index n of the grating is 1.5.

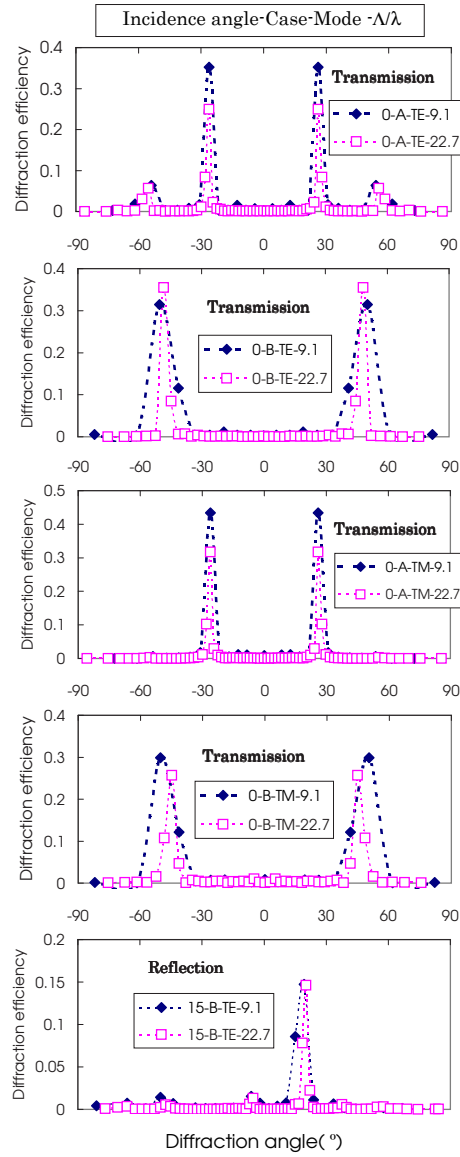


Fig. 2. (Color online) Angular distribution of the diffraction efficiency for different polarization and light directions. Λ/λ is 9.1 or 22.7. The aspect ratio is 1. Though the diffraction efficiency is discrete, it is connected with the auxiliary line to make it intelligible.

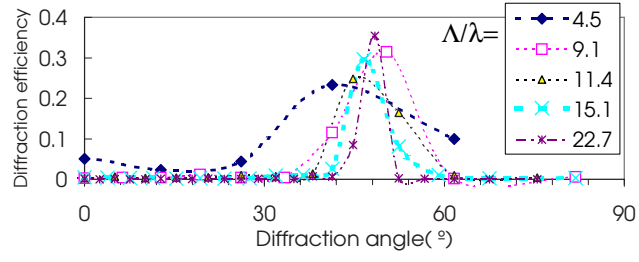


Fig. 3. (Color online) Angular distribution of the transmissive diffraction efficiency of the TE mode for case B for different Λ/λ . The aspect ratio is 1. The diffraction efficiency is connected with the auxiliary line to make it intelligible. Λ/λ is varied from 4.5 to 22.7.

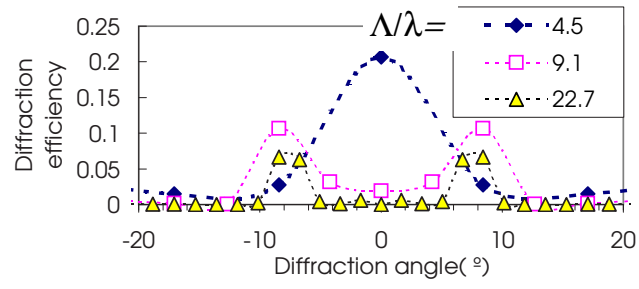


Fig. 4. (Color online) Angular distribution of the transmissive diffraction efficiency of the TE mode for case A for different Λ/λ . The aspect ratio is 2. The diffraction efficiency is connected with the auxiliary line to make it intelligible. Λ/λ is varied from 4.5 to 22.7.

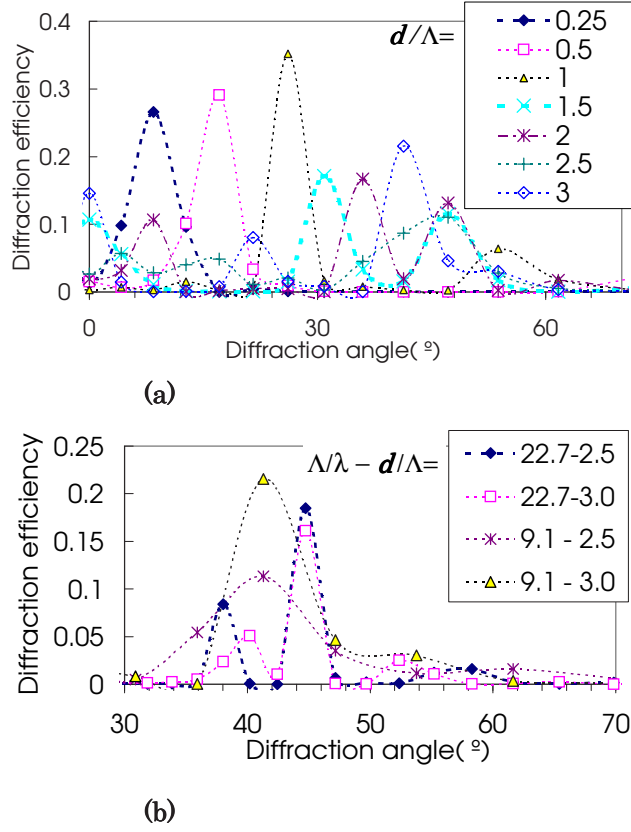


Fig. 5. (Color online) Angular distribution of the transmissive diffraction efficiency of the TE mode for different d/Λ for case A. The diffraction efficiency is connected with the auxiliary line to make it intelligible. (a) d/Λ is varied from 0.25 to 3. (b) d/Λ is 2.5 and 3, and Λ/λ is 9.1 and 22.7.

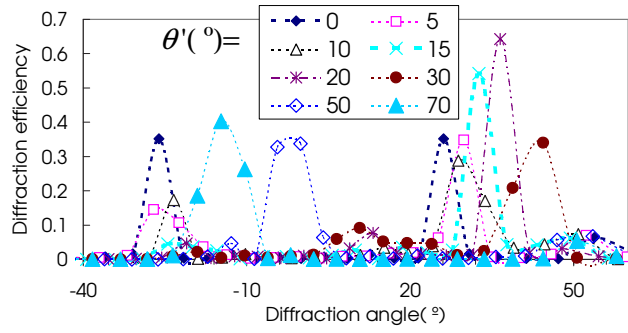


Fig. 6. (Color online) The incidence angle θ' is varied. The angular distribution of θ' from 0° to 30° and that of θ' from 50° to 70° may be attributed to different groups by their peak width.

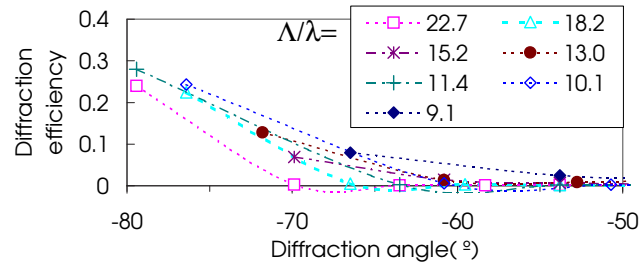


Fig. 7. (Color online) The angular distribution of the transmitted light is shown. The incidence angle is 20° , the direction of the incident light is case B, the polarization is TE, d/Λ is 1, and Λ/λ was varied. The angle of the peak is near 90° . The angular distribution varies greatly with Λ/λ .

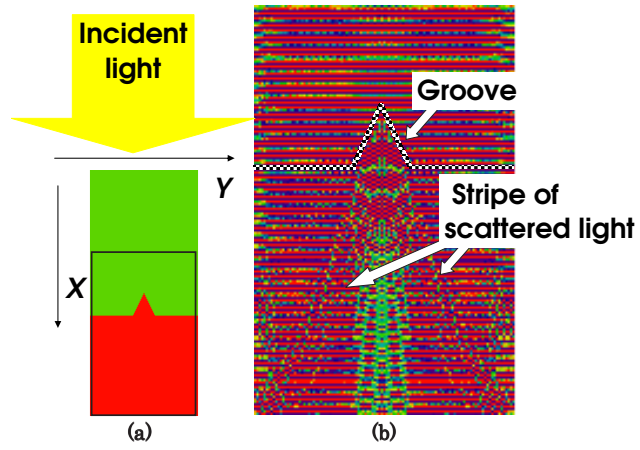


Fig. 8. (Color online) (a) The field for FDTD calculation and the grating. The black rectangular area is expanded into the area of (b). (b) The phase distribution of the scattered light in the TE mode and for case A. There is only one groove, unlike Fig. 1. The width of the groove is 9.1λ and the aspect ratio is 1.

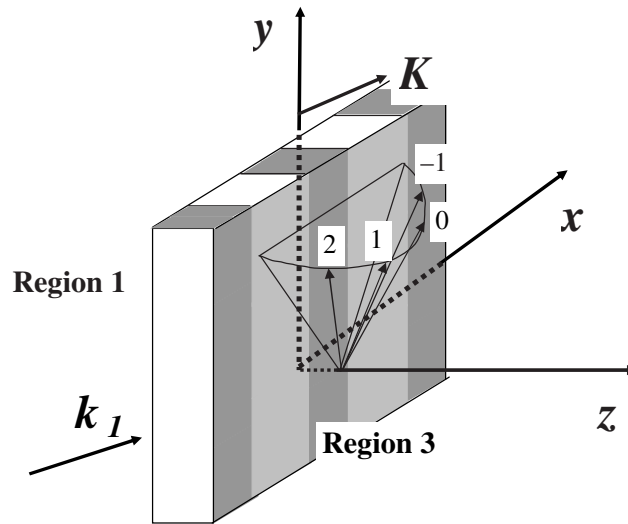
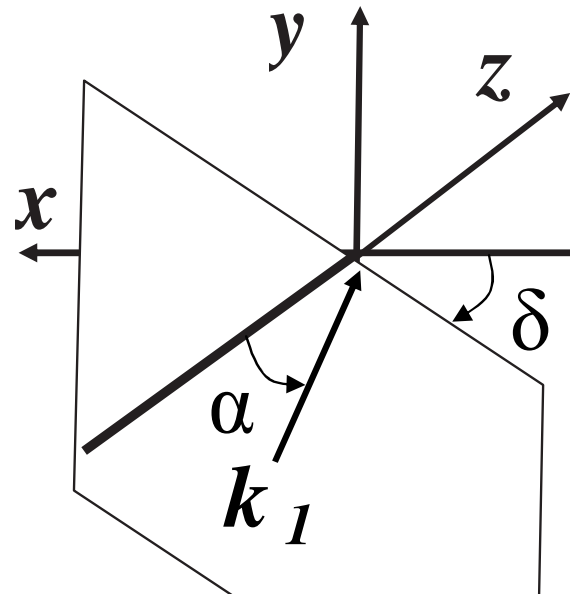


Fig. 9. Geometry of forward-diffracted wave vectors showing the conical nature of diffraction. Forward-diffracted waves ($i = -1$ to $i = +2$) are indicated by the arrow. The light travels from region 1 ($z < 0$) to region 3 ($z > d$).



Electromagnetic wave

Fig. 10. A linearly polarized electromagnetic wave of wave vector k_1

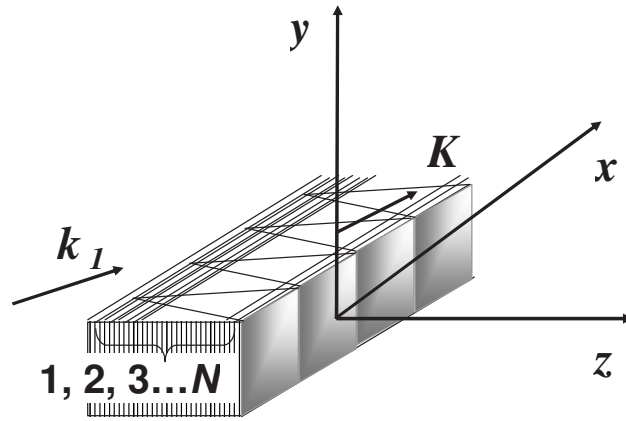


Fig. 11. The planar gratings resulting from the decomposition of the surface relief grating into N thin gratings.

Table 1. The results of curve fitting for Fig. 3 by the Fraunhofer single-slit diffraction pattern for different Λ/λ in case B. Apparent ratio of the period is calculated by $(\Lambda/\lambda)(\lambda_2/\Lambda_2)$.

Λ/λ	4.5	9.1	11.4	15.1	22.7
λ_2	1.65	0.7	0.6	0.43	0.3
$(\Lambda/\lambda)(\lambda_2/\Lambda_2)$	1.49	1.27	1.37	1.30	1.36
θ	43.3	48.3	47.2	47.2	47.6

Table 2. The results of curve fitting for Fig. 4 by Fraunhofer single-slit diffraction pattern for different Λ/λ and d/Λ in case A. The parameters are the same as in Fig. 1 and Eq. (1). The apparent ratio of the period is calculated by $(\Lambda/\lambda)(n\lambda_2/\Lambda_2)$.

Λ/λ	4.5	9.1	22.7
λ_2	1.05	0.54	0.22
$(\Lambda/\lambda)(n\lambda_2/\Lambda_2)$	1.42	1.47	1.50
θ	0	7.7	7.7

Table 3. The results of curve fitting for Fig. 5 by Fraunhofer single-slit diffraction pattern for different aspect ratios in case A. Λ/λ is 9.1. Apparent ratio of period is calculated by $(\Lambda/\lambda)(n\lambda_2/\Lambda_2)$.

d/Λ	0.25	0.5	1	1.5	2	2.5	3
λ_2	0.7	0.62	0.46	0.49	0.46	0.5	0.28
$(\Lambda/\lambda)(n\lambda_2/\Lambda_2)$	1.91	1.69	1.26	1.34	1.26	1.37	0.76
θ	8.4	16.4	26	31.1	35.9	43.3	42.2

Table 4. The results of curve fitting for Fig. 6 by Fraunhofer single-slit diffraction pattern for different incidence angle in case A. Apparent ratio of period is calculated by $(\Lambda/\lambda)(n\lambda_2/\Lambda_2)$.

θ'	0	5	10	15	20	30	50	70
λ_2	0.46	0.51	0.48	0.49	0.45	0.45	0.75	0.88
$(\Lambda/\lambda)(n\lambda_2/\Lambda_2)$	1.26	1.39	1.31	1.34	1.23	1.23	2.05	2.40
θ	26	29.9	32.7	31.1	36.5	41.8	-1.9	-14.8

Table 5. Total transmissivity of Fig. 7 as a function of Λ/λ .

Λ/λ	22.7	18.2	15.2	13.0	11.4	10.1	9.1
Transmissivity	0.57	0.46	0.30	0.39	0.62	0.62	0.33

^a“Transmissivity” is the sum of the transmission diffraction efficiency.